

Friedrich Schiller Universität Jena
PAF

Dissertation

High-Fluence Ion Beam Irradiation of Semiconductor Nanowires

Andreas Johannes

März 2015

Abstract

Hier alles Bla

Contents

1	Introduction	1
2	Background	2
2.1	Ion-solid interaction	2
2.2	Simulation of ion-solid interaction	8
3	Experimental Methods	10
3.1	Nanowire synthesis	10
3.2	Modification	12
3.3	Characterization	13
4	Summary and Outlook	18

1 Introduction

2 Background

This chapter will provide a general scientific context for this dissertation. First a general outline of energetic ion-solid interaction is given. Then the possibilities of simulating this ion-solid interaction are discussed with an emphasis on those effects that will be relevant to the experiment in this thesis.

2.1 Ion-solid interaction

Energy loss

An energetic ion impinging on a solid will lose its kinetic energy to the solid in a variety of processes. The stopping power S is well described for a large energy range by the Bethe (sometimes “Bethe-Bloch”) formula derived using the Born approximation perturbation theory on the impact between the ‘fast’ ion and the ‘slow’ electrons in the solid:

$$S = \frac{dE}{dx} = -A \cdot \frac{\rho Z_2 \cdot Z_1^2}{\beta^2} \cdot \left[\ln \left(\frac{B \cdot \beta^2}{Z_2 \cdot (1 - \beta^2)} \right) - \beta^2 \right], \quad (2.1)$$

with A and B positive combinations of constants, ρ the density and Z_2 the atomic number of the target, Z_1 and $\beta = v/c$ the atomic number and relativistic velocity of the ion. Corrections to this formula are especially necessary for low ion energies, but in detail they are dependent on the

2.1 Ion-solid interaction

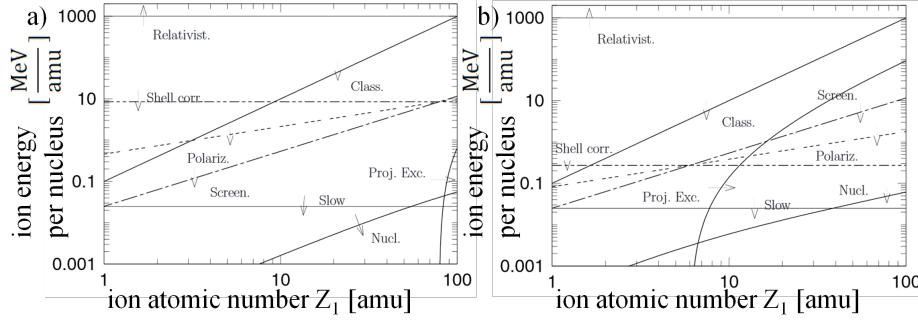


Figure 2.1: Illustration of the dominant effects on the stopping power for an ion of mass Z_1 and energy E in *Au* a) and *C* b). Adapted from [Sig04].

target composition, the ion energy and ion mass in a non-trivial way. Figure 2.1 and the following discussion illustrates stopping regimes and why corrections are required to the Bethe formula. It is adapted from [Sig04].

At high ion energies ($> 1 \text{ GeV}/\text{amu}$, labeled “Relativist.”) highly relativistic effects have to be taken into account. At these energies we have, for example, Cherenkov radiation. Typically, nuclear reactions and resonances also occur at high ion energies. They may play a role at lower energies, especially for light ion-target combinations. However, as nuclear reactions may change the ion species, their cross sections are usually treated separately from the stopping power.

The horizontal line labeled “Shell corr.” marks the Thomas-Fermi velocity ($Z_2^{2/3}v_0$) of the target electrons. The constant $v_0 = e^2/\hbar = 25 \text{ keV}/\text{amu}$ is the Bohr velocity. In the parameter-space below this line the ion is moving at speeds comparable to that of the electrons in the target. In the low energy area below the line labeled “Slow” ($25 \text{ keV}/\text{amu}$) the ion is traveling at speeds below the Bohr velocity of the target electrons. Here the ion velocity is only comparable to that of the valence electrons in the solid. Both these points mean that

2 Background

the actual electron density distribution and chemical nature of the solid becomes relevant, which is of course not considered in the general Bethe formula. This makes a general and accurate theoretical prediction of electronic stopping impossible for low ion energies. Specific ion-target combinations require specific investigations.

Above the line showing the Thomas-Fermi velocity of the ion ($v = Z_1^{2/3}v_0$, “Screen.”) the ion can be assumed to be stripped of all its electrons. Below, a screening function must consider the effective charge of the ion. Below the curve labeled “Proj. Ext.” the ion (projectile) carries a comparable number of electrons to the target making excitation processes in the electronic configuration of the ion significant.

For ion velocities $v < (Z_1Z_2)^{1/3}v_0$ (labeled “Polariz.”) a higher order (Z_1^3) correction term to the Bethe formula becomes relevant due to the Barkas-Andersen effect. Below the line marked “Class.” ($Z_1^2 \cdot 100 \text{ keV}/amu$) classical Bohr orbits can be used for electrons around the ion, this is a *sufficient* criterion for the derivation of the Bethe formula not a *necessary* one.

Finally, not be confused with the nuclear reactions already mentioned, in the region marked “Nucl.”, at low ion energies and for large ions, the interaction with the electronic system becomes weak. Here the contribution of the coulomb interaction between ion and individual target atoms as a whole become the main contribution to slowing the ion. This is called nuclear stopping in contrast to the electronic stopping discussed so far, as kinetic energy is transferred to the target nuclei, not just the electrons.

Those ion-solid interaction processes which are specific to the properties of the target material can be used to characterize the material. These methods are summarized as ion beam analysis (IBA). A confident and comprehensive review of the possibilities of IBA can be found in reference [JBB⁺12]. The effects that the ion irradiation has on the solid

will be discussed next by looking at the electronic and nuclear energy loss separately.

Discussion of electronic energy loss

Electronic stopping S_e “excites the electronic system”. In the simplest case a target atom is ionized, followed by a host of effects such as characteristic X-ray emission and Auger electron emission associated with the relaxation of this excited state. Analogously, excitation in a semiconductor is associated with band to band, exciton etc. recombination. Detection of these emissions can be used for IBA. The luminescent and fluorescent relaxation mechanisms are, however, generally not very efficient. Most of the energy deposited in the electronic system will be turned into kinetic energy of electrons and subsequently converted to heat. This happens very locally on the nm scale of the electrons mean free path and thus also very quickly, within the order of ps .

The effects of such local heating on a solid are diverse. Defects and amorphous regions may either appear or disappear, depending on the material and its history. For large ion masses and energies (swift, heavy ions), the deposited energy density becomes large enough to form an “ion track” around the path of the ion. Ion tracks are a whole field of research outlined well by references [TDP92, MK97, WKW04]. Very large electronic losses have to be treated carefully as a large percentage of the electrons within the track are energized and some electrons also gain a significant amount of kinetic energy.

The energies used in this dissertation are in the order of $\approx 100 keV$ with elements of mass $\approx 100 amu$. The energy regime investigated in this dissertation is thus right at the bottom of the area plotted in figure 2.1. Electronic stopping is not dominant so that it is sufficient to treat the electronic energy loss as a local heat source.

2 Background

Discussion of nuclear energy loss

The seemingly more straightforward process in the energetic ion-solid interaction is an elastic collision between the impinging ion and a target atom. Its first observation was in the famous Rutherford (Geiger–Marsden) experiment [Rut11] which was groundbreaking to understanding the structure of matter. Nuclear energy loss is caused by the kinetic energy which is transferred from the energetic ion onto an atom in the target. An impinging ion can transfer considerable energy to an atom, which in turn will collide with other lattice atoms, leading to the formation of a collision cascade. This displacement of atoms from their lattice position is the main contribution to irradiation damage and sputtering of the target.

The amorphization of crystalline semiconductors has been investigated extensively with a good review found in reference [WWS12]. The damage production depends a lot on the irradiated semi-conductor and on the density of the collision cascade caused by the irradiating ion. In general the defects produced by nuclear energy loss are Frenkel pairs. On further irradiation the Frenkel pairs can agglomerate to form extended defect clusters which initiate full amorphization. The fluence at which the material is amorphized is also highly temperature dependent as Frenkel pairs can anneal at high implantation fluences. This can lead to an arbitrarily high amorphization fluence, if the annealing of defects is faster than their creation. A typical ‘radiation hard’ material is ZnO which does not amorphize at even at $10^{17} \text{ cm}^{-2} \text{ Ar}^+$ irradiation at 15 K [WWS12]. An arbitrarily large amorphization threshold can also be obtained for Si irradiated with 300 keV Ar^+ at $300^\circ \text{ C} (\approx 600 \text{ K})$ [?].

In addition to the activation of defect recombination by increasing the ‘global’ temperature, an increased local temperature by the energy deposited by the ion will also lead to ‘dynamic annealing’. In a re-

2.1 Ion-solid interaction

cent study [TVM⁺15] the dynamic annealing was enhanced by the simultaneous irradiation with 36 MeV *W* a swift, heavy ion leading to predominantly electronic energy loss and 900 keV *I* leading to large nuclear losses. Simultaneous irradiation lead to much less damage in the irradiated *SiC* than subsequent irradiation. The reduction of structure sizes also leads to larger dynamic annealing as there is less material into which the energy deposited by the ion can dissipate. This was shown in the *Mn* irradiation of *GaAs* nanowires [Bor12, JHMR15] and could be used to improve the magnetic properties of the *GaAs* : *Mn* nanowires [BMB⁺11, PKB⁺12, KPJ⁺13, PKJ⁺14].

A typical assumption in the theoretical treatment of nuclear energy loss is the binary collision approximation (BCA) for the ion and the target atom. Under this assumption nuclear stopping is treated as a series of collisions between single particles. With the additional assumptions of 1) a spherically symmetric interaction potential and 2) the neglect of possible electronic effects (chemical binding) between the collision partners, the angular-momentum is conserved in the collision and the classical scattering-integrals can be solved.

The resulting trajectories of a *Si* – *Si* collision at 10 eV is plotted in figure 2.2. The large difference between the Molière screened Coulomb potential and the *Si* – *Si* potential derived by Dirac-Fock-Slater code is clearly visible. The former is a purely repulsive Coulomb interaction, while the latter includes an attractive interaction for large interatomic distances similar to the well known Lennard-Jones potential [Eck91]. For high energy collisions a “universal” ZBL potential based on Coulomb interaction is quite successful [ZLB85], however for low energy collisions a generalized formula cannot be accurate and specific potentials have to be developed for each combination of collision partners [Ded95, NRS97, ANNK02, ND08].

2 Background

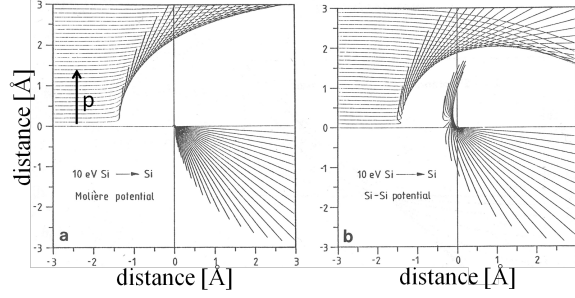


Figure 2.2: Trajectories of a 10 eV $Si - Si$ collision for a) Molière and b) $Si - Si$ potential. The trajectories end after the same elapsed time for each impact parameter p . Adapted from [Eck91].

In addition to this problem of finding the correct interaction potential for a collisions, depending on the ion and the atomic structure of the irradiated material, the collision parameters relevant to low energy collisions are within the order of the inter-atomic distance of a few Å, see figure 2.2. The assumption, that this is still a binary collisions can thus no longer be valid. In conclusion, it has to be noted that similar to the electronic stopping case, the assumptions for a generalized treatment of nuclear stopping are well fulfilled for large ion energies, but lose their validity at low energies $\ll 1 \text{ keV}$.

Sputtering

A prominent role in this dissertation will be played by a special effect of nuclear energy loss arising when the path of the recoiled atom intersects the targets surface: sputtering. The foundation of sputter theory was laid by Sigmund [?]. It is outlined in the following. The nuclear stopping of ions leads to the formation of highly branched collision cascades. Therefore, the majority of recoiled atoms is found at the end of the many branches. Because of this, the majority of sputtered particles has a low energy and thus a low range in the material [?]. They must

2.1 Ion-solid interaction

thus originate from the surface of the target and the sputter yield, as the number of atoms sputtered per impinging ion, can be estimated by calculating the nuclear energy loss at the surface of the irradiated material and dividing it by a factor to account for the probability of the atom leaving the solid.

The probability for the atom to leave the solid includes geometric considerations and the ‘surface binding energy’ (SBE). A reasonable model for the SBE is that of a potential plateau with the height of the enthalpy of sublimation which has to be overcome by the atom approaching the surface. This equates the energy required for sputtering an atom to the thermal energy required for sublimation. The SBE model for sputtering neglects all effects related to the directionality of the local binding forces experienced by the atom to be sputtered and the modification of the surface by repeated removal of atoms.

A reasonable assumption for the nuclear energy deposition distribution is to be a Gaussian ellipsoid, with the center at the ion range and the longitudinal and lateral straggling naturally defining its extensions. This approach was used by Sigmund to arrive at a good explanation for the energy dependence of sputtering from flat surfaces. Starting at low energies, the sputter yield will initially increase with increasing energy, simply due to more energy being available. For further increasing energy, however, the ion range becomes larger, leading to a predominant deposition of the energy deeper inside the target, away from the surface. A maximum is thus found at energies where the ion range is in the order of the longitudinal straggling.

Applications of this theory have been made to more complex surfaces. The Bradley-Harper theory of ripple formation on ion irradiated planes relies on the anisotropic sputtering predicted by the Sigmund model applied to a structured surface [?]. Also recent investigations on sputtering of spherical [?] and cylindrical [?] nanostructures have compared their

2 Background

results with that predicted by the Sigmund model and found it to be a decent first approximation.

2.2 Simulation of ion-solid interaction

In practice the theory of ion-solid interaction is implemented in simulation tools which allow the experimenter to predict experimental outcomes. The most frequent example is obtaining the energy dependence of the ion range by simulations and using that information to decide which energy and fluence of irradiation is needed to obtain a desired doping concentration. On a deeper level, an experimentally observed behavior can be understood better by comparing it with simulation including different effects. The two main simulation approaches used to simulate the ion solid interaction are Monte-Carlo (MC) and Molecular Dynamic simulations (MD).

Monte-Carlo and the binary collision approximation

BCA, MC Ausgiebige Verwendung von *iradina* [BR11]

Molecular dynamic simulations

MD general: cite Alder, Nordlund+Kuronen

3 Experimental Methods

The respective machines, technologies and concepts used within this dissertation can not be fully characterized within a couple of pages. This section will mainly serve as a glossary of the methods, abbreviations and acronyms used in the following dissertation which not every reader may be familiar with. Further, only an incomplete collection of references to textbooks and literature can be given.

3.1 Nanowire synthesis

Nanostructures can generally be synthesis can be categorized according to two approaches: “bottom-up” and “top-down”. The “bottom-up” approach relies on the self-organized arrangement of matter using an inherent anisotropy in one of the thermodynamic properties of the relevant system to create nanoscale structures. Depending on the material, crystal quality, morphology, infrastructure requirements, the quantity to be produced etc. there is a large variety of processes available for synthesis. For semiconductor nanowires the main approaches developed are based on hydro-thermal, pyrolytic, vapor-transport, chemical vapor deposition, laser ablation, metal organic vapor phase epitaxy (MOVPE), molecular beam epitaxy (MBE) processes, in ascending order of complexity, or number of controllable parameters.

3 Experimental Methods

A very common mechanism to create the anisotropy required to get the one dimensional growth required to obtain nanowires is the vapor-liquid-solid growth (VLS) first described by Wagner and Ellis. The variety of processes listed before are responsible to provide the ‘vapor’ of material for this growth mechanism. With vapor transport the source material eg. ZnO is simply evaporated in a typically inert atmosphere and transported within an oven to the substrate by diffusion or gas flow. Chemical vapor deposition uses reactive gases such as SiH_3 to provide the material, in this case Si in a temperature and pressure controlled oven. Similarly in MOVPE a metal-organic gas is used as at least one of the sources. For example TMG (trimethylgallium) and AsH_3 to grow $GaAs$.

Although also self-catalyzed growth has been observed, the liquid part in VLS is typically played by a metal catalyst deposited on the growth substrate. The material in the vapor phase can collect in the catalyst droplet until the concentration is saturated. Preferential segregation of the nanowire material at the droplet-substrate interface leads to the growth of a wire. The size of the droplet can be used to control the diameter of the grown nanowire to some extent. ZnO [BMS⁺06, Sti08, Mü09, Ogr13], $GaAs$ [BDSS04, WDJ⁺09] and Si [LSH⁺08] nanowires investigated in this dissertation where grown with the VLS mechanism using vapor transport, MOVPE and chemical vapor deposition respectively. An epitaxial relation between the substrate and the nanowire material may be used to direct the growth. Typical nanowire diameters and lengths are $50 - 300\text{ nm}$ and $> 10\text{ }\mu\text{m}$ respectively.

Nanowires can also be synthesized “top-down”. A “top-down” approach requires a predefined template which is used to control the desired morphology. The Si -nanowire arrays investigated within this dissertation were etched by reactive ion etching (RIE) through a circular Ni hard-mask which defined the nanowire diameter *cite NL*. The

“top-down” etching process was used, as with it it is possible to prepare nanowires with diameters varying from 50 nm to $2\text{ }\mu\text{m}$ with a height of $\approx 3\text{ }\mu\text{m}$ on a single substrate.

Since the growth itself was performed mainly by collaborators in Lund University (*GaAs*) and TU Vienna (*Si*) and is not part of the investigations reported here, the inclined reader is redirected to the the cited references for further details respective growth parameters and their investigation.

3.2 Modification

ROMEIO

The ion irradiation for this dissertation was performed at the general purpose HVE implanter “ROMEIO” at the IFK in Jena. It can provide an ion beam of virtually any element at energies of $10 - 380\text{ keV}$. The beam passes a 90° selector magnet and can be swepted with a frequency of kHz to homogeneously irradiate areas up to several tens of cm^2 with ion currents of up to 1 mA . For this work ion current densities were limited to 500 nA/cm^2 or 10^{16} ions/cm^2 in 15 min . As previous work has shown that the irradiation of nanowires can bend the nanowires [BSL⁺11, Bor12], a rotatable and heatable, tilted stage (RHT) was custom built [Noa14]. With it bending of the nanowires grown upstanding on a substrate can be avoided as they are irradiated homogeneously from all sides at an angle of 45° . All the samples investigated in this thesis were rotated on the RHT and its preceding prototype sample stages during the irradiation.

3 Experimental Methods

FIB

Some sample preparation required a focused-ion-beam (FIB). FIBs are highly specialized ion accelerators where the main objective is to obtain a small ion beam focus. The most wide spread systems use a Ga^+ beam and acceleration voltages up to 30 keV . The main use for FIBs is to use the focused ion beam to sputter material extremely locally, making it a versatile tool for nano-machining. The FEI DualBeam Helios NanoLab 600i FIB system used for this dissertation is a scanning electron microscope (SEM) - FIB combination, so that the sample can be milled with the ion beam and investigated with the SEM. It also is equipped with a Pt -metal-organic-gas injection system. The Pt containing organic gas can be cracked locally on the sample by the secondary electrons created by either the electron or the ion beam. Most of the Pt is deposited near the impact point of the primary beam and the substrate, however typically a rather large ‘halo’ of minor Pt deposition can extend for a couple of μm . The FIB system can thus deposit and mill structures on a nm scale.

3.3 Characterization

SEM

The morphological changes in the nanowires were characterized by high resolution SEM in the FEI DualBeam Helios NanoLab 600i focused-ion beam system. The spacial resolution of the SEM system is $\approx 2\text{ nm}$. To quantify the sputtering images of individual nanowires were made before and after ion irradiation. To find exactly the same place on the sample, a series of images with increasing magnification has to be made. Typically images were made at an angle of 45° to the substrate with the substrate aligned the same way before and after irradiation.

3.3 Characterization

An semi-automated image analysis protocol was developed by Stefan Noack in his Master thesis [Noa14, ?] to evaluate the SEM images of a large number of nanowires. It applies a (3x3) median filter to smoothed out some noise and a Gaussian unsharp mask with $\sigma = 1\text{ px}$ and weighted at 60 % to resharpened the edges [San04]. An Otsu threshold [Ots79] is applied to separate the lighter nanowire from the darker background. Next, open source particle analysis software is used to find the main body of the nanowire and turn the it upright, correcting for any marginal tilt remaining in the SEM images [SACF⁺12, SPTS12]. Finally the sum of the gray-values in each line used to calculate the diameter at that height along the nanowire axis. As the investigated nanowires showed a characteristic bulge at the base, this point can be used to align the height profiles of a single wire before and after irradiation.

EBSD

Electron back-scatter diffraction (EBSD) was used to identify whether nanowires remained crystalline after irradiation with a Carl Zeiss Auriga CrossBeam Workstation. EBSD can be measured with a large CCD detector in a SEM. The electron beam is focused on the sample at an arbitrary angle. Electrons are scattered from the sample lattice and the scattered electrons are detected by the CCD detector. Bragg diffraction along the crystal lattice planes produces a characteristic pattern of Kikuchi lines on the detector [Kik28, FH13] in crystalline samples. Amorphous or nano-crystalline samples show no pattern.

nano-XRF

The most experimentally advanced characterization method was X-ray fluorescence with a nano-focussed X-ray beam (nano-XRF) at the European Synchrotron Radiation Facility (ERSF), beamlines ID16b and

3 Experimental Methods

ID13. Hard X-ray radiation will excite the atoms within a radiated material to emit characteristic X-ray radiation. This X-ray fluorescence can be detected in an energy dispersive semiconductor detector and used to identify and quantify the elements in the sample. In principle the method is similar to the more wide-spread energy dispersive X-ray spectroscopy (EDX), where the electron beam is used to excite characteristic X-ray fluorescence. Very good lateral resolution can be obtained by having an EDX detector in an SEM. The advantage of using X-rays lies in the absence of this Bremsstrahlung which high energy electrons in matter produce in addition to the characteristic X-rays. In XRF there is thus a much lower background and a much lower concentrations of elements can still be detected and quantified. Unlike normal characteristic X-ray tubes, synchrotron radiation is typically very brilliant, allowing it to be focused. The beamlines ID16b and ID13 were run at various energies above 16 keV and a focus of typically $\approx 80\text{ nm}$ and $\approx 250\text{ nm}$ respectively. The nano-XRF thus allows for quantification of low concentrations with sufficient lateral resolution to resolve axial concentration gradients in a nanowire. Unfortunately, the resolution is not good enough to investigate radial distributions.

At both beamlines the nanowires are scanned under the fixed focal point of the X-ray beam with piezo-motors while the XRF spectra are collected with a Vortex EM silicon drift X-ray detector. The investigated *Mn* irradiated *ZnO* nanowires were deposited on TEM grids either randomly by ‘imprinting’ or individually by using the mico-manipulator in the FEI DualBeam FIB. Transferring individual wires requires some finesse, but it is possible to detach the *ZnO* nanowires from their substrate without the *Ga* FIB and to place them on the “lacey-carbon” TEM Grids without any additional *Pt* deposition. In this way SEM images before and after irradiation of the same wire investigated by nano-XRF are available.

3.3 Characterization

The spectra used for quantification were obtained in multiple scans across a nanowire at regular intervals along the nanowire's length. As the XRF signal can be used to locate the nanowire, only the points near the nanowire were measured with a high integration time and a low step-width ($< \frac{1}{2}$ focal spot) to ensure a large number of counts ($> 10^5$ per scan) at reasonable measuring times.

nano-XRF quantification

Spectra were evaluated using the open source PyMCA software package [SPC⁺07]. The effects of self absorption and excitation can be neglected, as the investigated nanowires are very thin compared to the absorption length of a couple of μm of hard X-rays. However, the detector-sample distance is an unavoidable attenuation length in air, with its absorption by the heaviest element in air, *Ar*. As the element investigated, *Mn*, is relatively light, its characteristic X-ray emission at $K_{\alpha, Mn} = 5.9 keV$ suffers more absorption than the heavier *Zn* with $K_{\alpha, Zn} = 8.6 keV$. Thus absorption of the XRF signal in air has to be considered carefully in the fitting with PyMCA. The accuracy was double checked by measuring and quantifying trace elements in a calibration sample of bovine liver. In this way optimal fitting parameters were found and applied to all measured spectra in the PyMCA batch mode. Oxygen can not be quantified in these beamlines, as the signal is attenuated too far. The quantification of the *Mn* content in the *ZnO* nanowires thus relies on the assessment of the *Mn/Zn* ratio. It is a decent approximation to assume that the *ZnO* remains stoichiometric even during the irradiation. The samples are irradiated in a chamber with a base pressure $\approx 10^{-6} mbar$, so according to the Hertz-Knudsen equation this will give a coverage of roughly one mono-layer or $10^{15} particles/cm^2s$. The maximum ion current density of $500 nA/cm^2s$ amounts to $10^{13} ions/cm^2s$, so that an unlikely amount of

3 *Experimental Methods*

preferential sputtering would be required to deplete the oxygen out of the wires. In any case, the wires will be oxidized in the normal atmosphere post irradiation. The Mn/Zn ratio is thus a good proxy for the Mn concentration.

The quantification limit can be tested within PyMCA by finding an appropriate photon flux and nanowire interaction volume for a simulation to reproduce the XRF spectrum with the actually measured number of counts at $K_{\alpha,Zn}$. The Mn content in the simulated matrix can then be decreased until the minimum Mn content is found which gives a signal at $K_{\alpha,Mn}$ just above the actually measured noise level. In this way a lower limit for the concentration resolution can be found at typically $0.1\% Mn/Zn$.

4 Summary and Outlook

check: Master Thesis Noack, Ogrisek, Conference proceeding D. Sage, Rutherford

Bibliography

- [ANNK02] Karsten Albe, Kai Nordlund, Janne Nord, and Antti Kuro-
nen. Modeling of compound semiconductors: Analytical
bond-order potential for Ga, As, and GaAs. *Physical Re-
view B*, 66(3):035205, July 2002.
- [BDSS04] M. Borgström, K. Deppert, L. Samuelson, and W. Seifert.
Size- and shape-controlled GaAs nano-whiskers grown by
MOVPE: a growth study. *Journal of Crystal Growth*,
260(1–2):18–22, January 2004.
- [BMB⁺11] Christian Borschel, Maria E. Messing, Magnus T.
Borgstrom, Waldomiro Paschoal, Jesper Wallentin, Sandeep
Kumar, Kilian Mergenthaler, Knut Deppert, Carlo M.
Canali, Hakan Pettersson, Lars Samuelson, and Carsten
Ronning. A New Route toward Semiconductor Nanospin-
tronics: Highly Mn-Doped GaAs Nanowires Realized
by Ion-Implantation under Dynamic Annealing Condi-
tions. *Nano Letters*, 11(9):3935–3940, September 2011.
WOS:000294790200073.
- [BMS⁺06] C. Borchers, S. Müller, D. Stichtenoth, D. Schwen, and
C. Ronning. Catalyst Nanostructure Interaction in the
Growth of 1d ZnO Nanostructures. *The Journal of Phys-
ical Chemistry B*, 110(4):1656–1660, February 2006.

Bibliography

- [Bor12] Christian Borschel. *Ion-Solid Interaction in Semiconductor Nanowires*. PhD thesis, University Jena, Jena, 2012.
- [BR11] C. Borschel and C. Ronning. Ion beam irradiation of nanostructures – A 3d Monte Carlo simulation code. *Nuclear Instruments and Methods in Physics Research Section B: Beam Interactions with Materials and Atoms*, 269(19):2133–2138, October 2011.
- [BSL⁺11] Christian Borschel, Susann Spindler, Damiana Leroose, Arne Bochmann, Silke H. Christiansen, Sandor Nietzsche, Michael Oertel, and Carsten Ronning. Permanent bending and alignment of ZnO nanowires. *Nanotechnology*, 22(18):185307, May 2011. WOS:000288653300010.
- [Ded95] Gv Dedkov. The Interatomic Interaction Potentials in Radiation Physics. *Physica Status Solidi a-Applications and Materials Science*, 149(2):453–513, June 1995. WOS:A1995RH61400001.
- [Eck91] Wolfgang Eckstein. *Computer Simulation of Ion-Solid Interactions*. Springer Berlin Heidelberg, Berlin, Heidelberg, 1991.
- [FH13] Brent Fultz and James Howe. *Transmission Electron Microscopy and Diffractometry of Materials*. Graduate Texts in Physics. Springer Berlin Heidelberg, Berlin, Heidelberg, 2013.
- [JBB⁺12] C. Jeynes, M. J. Bailey, N. J. Bright, M. E. Christopher, G. W. Grime, B. N. Jones, V. V. Palitsin, and R. P.

Bibliography

- Webb. "Total IBA" - Where are we? *Nuclear Instruments & Methods in Physics Research Section B-Beam Interactions with Materials and Atoms*, 271:107–118, January 2012. WOS:000299986500018.
- [JHMR15] Andreas Johannes, Henry Holland-Moritz, and Carsten Ronning. Ion beam irradiation of nanostructures: sputtering, dopant incorporation, and dynamic annealing. *Semiconductor Science and Technology*, 30(3):033001, March 2015.
- [Kik28] Seishi Kikuchi. Diffraction of Cathode Rays by Mica. *Proceedings of the Imperial Academy*, 4(6):271–274, 1928.
- [KPJ⁺13] Sandeep Kumar, Waldomiro Paschoal, Andreas Johannes, Daniel Jacobsson, Christian Borschel, Anna Pertsova, Chih-Han Wang, Maw-Kuen Wu, Carlo M. Canali, Carsten Ronning, Lars Samuelson, and Håkan Pettersson. Magnetic Polarons and Large Negative Magnetoresistance in GaAs Nanowires Implanted with Mn Ions. *Nano Letters*, 13(11):5079–5084, 2013.
- [LSH⁺08] A. Lugstein, M. Steinmair, Y. J. Hyun, G. Hauer, P. Pongratz, and E. Bertagnolli. Pressure-induced orientation control of the growth of epitaxial silicon nanowires. *Nano Letters*, 8(8):2310–2314, August 2008. WOS:000258440700034.
- [Mü09] Sven Müller. *Structural and optical impact of transition metal implantation into zinc oxide single crystals and nanowires*. PhD thesis, Georg-August Universität Göttingen, Göttingen, 2009.
- [MK97] Antonio Miotello and Roger Kelly. Revisiting the thermal-spike concept in ion-surface interactions. *Nuclear Instru-*

ments and Methods in Physics Research Section B: Beam Interactions with Materials and Atoms, 122(3):458–469, February 1997.

- [ND08] Kai Nordlund and Sergei L. Dudarev. Interatomic potentials for simulating radiation damage effects in metals. *Comptes Rendus Physique*, 9(3–4):343–352, April 2008.
- [Noa14] Stefan Noack. *Sputter Effects of Silicon Nanowires under Ion Bombardment*. University Jena, Master Thesis, 2014.
- [NRS97] K. Nordlund, N. Runeberg, and D. Sundholm. Repulsive interatomic potentials calculated using Hartree-Fock and density-functional theory methods. *Nuclear Instruments & Methods in Physics Research Section B-Beam Interactions with Materials and Atoms*, 132(1):45–54, October 1997. WOS:A1997YF32200007.
- [Ogr13] Matthias Ogrisek. *Kontrolliertes Wachstum von Zinkoxid und Vanadium(IV)-oxid Nanodrähten*. University Jena, Master Thesis, 2013.
- [Ots79] NOBUYUKI Otsu. A Threshold Selection Method from Gray-Level Histograms. *IEEE Transactions on Systems, Man, and Cybernetics*, 9(1):62–66, 1979.
- [PKB⁺12] Waldomiro Paschoal, Sandeep Kumar, Christian Borschel, Phillip Wu, Carlo M. Canali, Carsten Ronning, Lars Samuelson, and Hakan Pettersson. Hopping Conduction in Mn Ion-Implanted GaAs Nanowires. *Nano Letters*, 12(9):4838–4842, September 2012. WOS:000308576000069.

Bibliography

- [PKJ⁺14] W. Paschoal, Sandeep Kumar, D. Jacobsson, A. Johannes, V. Jain, C. M. Canali, A. Pertsova, C. Ronning, K. A. Dick, L. Samuelson, and H. Pettersson. Magnetoresistance in Mn ion-implanted GaAs:Zn nanowires. *Applied Physics Letters*, 104(15):153112, April 2014. WOS:000335145200060.
- [PMB04] Lourdes Pelaz, Luis A. Marqués, and Juan Barbolla. Ion-beam-induced amorphization and recrystallization in silicon. *Journal of Applied Physics*, 96(11):5947–5976, December 2004.
- [Rut11] E Rutherford. The scattering of alpha and beta particles by matter and the structure of the atom. *Philosophical Magazine Series 6*, 21(125):669–688, May 1911.
- [SACF⁺12] Johannes Schindelin, Ignacio Arganda-Carreras, Erwin Frise, Verena Kaynig, Mark Longair, Tobias Pietzsch, Stephan Preibisch, Curtis Rueden, Stephan Saalfeld, Benjamin Schmid, Jean-Yves Tinevez, Daniel James White, Volker Hartenstein, Kevin Eliceiri, Pavel Tomancak, and Albert Cardona. Fiji: an open-source platform for biological-image analysis. *Nature Methods*, 9(7):676–682, June 2012.
- [San04] B Sankur. Survey over image thresholding techniques and quantitative performance evaluation. *Journal of Electronic Imaging*, 13(1):146, January 2004.
- [Sig04] Peter Sigmund, editor. *Stopping of Heavy Ions*, volume 204 of *Springer Tracts in Modern Physics*. Springer Berlin Heidelberg, Berlin, Heidelberg, 2004.
- [SPC⁺07] V. A. Solé, E. Papillon, M. Cotte, Ph. Walter, and J. Susini. A multiplatform code for the analysis of energy-dispersive

- X-ray fluorescence spectra. *Spectrochimica Acta Part B: Atomic Spectroscopy*, 62(1):63–68, January 2007.
- [SPTS12] Daniel Sage, D. Prodanov, J.-Y. Tinevez, and J. Schindelin. ImageJ User & Developer Conference (IUDC’12). 2012.
- [Sti08] Daniel Stichtenoth. *Dimensionseffekte in Halbleiternanodrähten*. PhD thesis, Georg-August Universität Göttingen, Göttingen, 2008.
- [TDP92] M. Toulemonde, C. Dufour, and E. Paumier. Transient thermal process after a high-energy heavy-ion irradiation of amorphous metals and semiconductors. *Physical Review B*, 46(22):14362–14369, December 1992.
- [TVM⁺15] Lionel Thome, Gihan Velisa, Sandrine Miro, Aurelien Debelle, Frederico Garrido, Gael Sattonnay, Stamatis Mylonas, Patrick Trocellier, and Yves Serruys. Recovery effects due to the interaction between nuclear and electronic energy losses in SiC irradiated with a dual-ion beam. *Journal of Applied Physics*, 117(10):105901, March 2015. WOS:000351442900074.
- [WDJ⁺09] Brent A. Wacaser, Kimberly A. Dick, Jonas Johansson, Magnus T. Borgström, Knut Deppert, and Lars Samuelson. Preferential Interface Nucleation: An Expansion of the VLS Growth Mechanism for Nanowires. *Advanced Materials*, 21(2):153–165, January 2009.
- [WKW04] W. Wesch, A. Kamarou, and E. Wendler. Effect of high electronic energy deposition in semiconductors. *Nuclear Instruments & Methods in Physics Research Section B-Beam*

Bibliography

Interactions with Materials and Atoms, 225(1-2):111–128, August 2004. WOS:000223792600010.

- [WWS12] W. Wesch, E. Wendler, and C. S. Schnohr. Damage evolution and amorphization in semiconductors under ion irradiation. *Nuclear Instruments and Methods in Physics Research Section B: Beam Interactions with Materials and Atoms*, 277:58–69, April 2012. 00009.
- [ZLB85] J. F. (James F.) Ziegler, U. Littmark, and J. P. Biersack. *The stopping and range of ions in solids / J.F. Ziegler, J.P. Biersack, U. Littmark*. The Stopping and ranges of ions in matter ; v. 1. Pergamon, New York, 1985. Includes index. Bibliography: p. 308-315.